

Article

Influence of High Conductive Magnetite Impurity on the Electrical Conductivity of Dry Olivine Aggregates at High Temperature and High Pressure

Lidong Dai ^{1,*}, Haiying Hu ^{1,*}, Wenqing Sun ¹, Heping Li ¹, Changcai Liu ^{1,2} and Mengqi Wang ^{1,2}

¹ Key Laboratory of High-temperature and High-pressure Study of the Earth's Interior, Institute of Geochemistry, Chinese Academy of Sciences, Guiyang, Guizhou 550002, China; sunwenqing@vip.gyig.ac.cn (W.S.); hepingli_2007@hotmail.com (H.L.); liuchangcai@vip.gyig.ac.cn (C.L.); wangmengqi@vip.gyig.ac.cn (M.W.)

² University of Chinese Academy of Sciences, Beijing 100039, China

* Correspondence: dailidong@vip.gyig.ac.cn (L.D.); huhaiying@vip.gyig.ac.cn (H.H.); Tel.: +86-851-85559715 (L.D.)

Received: 27 December 2018; Accepted: 11 January 2019; Published: 13 January 2019



Abstract: The electrical conductivity of dry sintered olivine aggregates with various contents of magnetite (0, 3, 5, 7, 10, 20, and 100 vol. %) was measured at temperatures of 873–1273 K and a pressure of 2.0 GPa within a frequency range of 0.1–10⁶ Hz. The changes of the electrical conductivity of the samples with temperature followed an Arrhenius relation. The electrical conductivity of the sintered olivine aggregates increased as the magnetite-bearing content increased, and the activation enthalpy decreased, accordingly. When the content of interconnected magnetite was higher than the percolation threshold (~5 vol. %), the electrical conductivity of the samples was markedly enhanced. As the pressure increased from 1.0 to 3.0 GPa, the electrical conductivity of the magnetite-free olivine aggregates decreased, whereas the electrical conductivity of the 5 vol. % magnetite-bearing sample increased. Furthermore, the activation energy and activation volume of the 5 vol. % magnetite-bearing sintered olivine aggregates at atmospheric pressure were calculated to be 0.16 ± 0.04 eV and −1.50 ± 0.04 cm³/mole respectively. Due to the high value of percolation threshold (~5 vol. %) in the magnetite impurity sample, our present results suggest that regional high conductivity anomalies in the deep Earth's interior cannot be explained by the presence of the interconnected magnetite-bearing olivine aggregates.

Keywords: electrical conductivity; magnetite; olivine aggregates; percolation threshold; high temperature and high pressure

1. Introduction

To explain the anomalous high conductivity in geophysical field observations of magnetotelluric and geomagnetic deep sounding data, many in situ laboratory-based high-pressure conductivity studies have been reported for relevant minerals and rocks in recent decades. Some potential explanations for high conductivity anomalies in the deep interior of the Earth and other planets have been proposed such as the hydrogen-bearing of nominally anhydrous minerals [1,2], dehydration of minerals [3,4], partial melting [5,6], dehydrogenation of minerals [7], anisotropy [8], and the presence of an interconnected high conductivity impurity phase [9].

In most available mineralogical models, olivine occupies a volume percentage in the range of 50–60% of the upper mantle. Many high-pressure experimental studies on the presence of interconnected high conductivity impurity phases have suggested that impurities such as ferrous

sulfide (FeS), graphite, and magnetite, can enhance the electrical conductivity of olivine at high temperatures and high pressures. [9–13]. Usually, these high conductivity impurity phases are widely distributed at grain boundaries, corners, and edges of polycrystalline olivine aggregates. Yoshino et al. [9] studied the electrical conductivities of FeS-bearing olivine with contents of 0, 3, 6, and 13 vol. % over a wide temperature range from 298 to 1673 K, at 3.0 GPa using a multi-anvil high-pressure apparatus. The magnitude of the percolation threshold in the molten iron–sulfur compounds in solid olivine was close to ~5 vol. %. Subsequently, Watson et al. [10] used piston cylinder high-pressure equipment to determine the grain interior and grain boundary electrical conductivities of polycrystalline San Carlos olivine with carbon-bearing and FeS-bearing impurities at 1.0 GPa and 623–1473 K. They found that impurity materials at the sample grain boundaries, corners, and edges, were present at a relatively low weight percentage of 0.1 wt. % (~0.16 vol. %) carbon, and a volume percentage of 1 vol. % (~1.4 wt. %) sulfide. These impurities increased the electrical conductivity of polycrystalline olivine by several orders of magnitude. Wang et al. [11] measured electrical conductivities of magnesite-bearing and graphite-bearing olivine aggregates at 1173–1673 K and 4 GPa using the multi-anvil high-pressure apparatus. The authors found that a ~1 wt. % (or higher) concentration percolation threshold for olivine aggregates might result in some of the observed high conductivity regions in the deep Earth’s interior. Recently, Zhang and Pommier [12] investigated the electrical conductivity of layered metal-bearing polycrystalline olivine aggregates with different ratios of metallic compositions (e.g., Fe, FeS, FeSi₂, and Fe–Ni–S–Si) at 5.0–6.0 GPa and temperatures up to 1948 K. They discussed the electrical conductivity anomalies of the core–mantle boundary and the outermost core of Mercury in detail. For magnetite-bearing impurities, there has been only one report on the electrical conductivity of a sintered solid solution of fayalite and magnetite (Fe_{3–δ}Si_δO₄, where δ = 0, 0.052, 0.085, 0.107, 0.169, and 0.288) by Yamanaka et al. [13] over an ultralow temperature range of 80–300 K, at atmospheric pressure, and under dry He gas flow conditions. They identified a mixed conduction mechanism based on both small polaron hopping and silicon vacancies at octahedral site operating in a Fe_{3–δ}Si_δO₄ solid solution of olivine. Previous mineralogical, petrological, and geochemical studies have shown that magnetite, with an inverse spinel structure, is intergrown with or exsolved from olivine in a variety of geotectonic environments [14,15]. As a representative high conductive impurity phase for magnetite, there is no any related data to be reported for the influence of magnetite content on the electrical conductivity of olivine to date.

In this work, we examine the electrical conductivities of dry magnetite-free and 5 vol. % magnetite-bearing olivine aggregates over the temperature range of 873–1273 K and pressures of 1.0–3.0 GPa, and with various magnetite volume percentages of 3, 5, 7, 10, 20, and 100 at 2.0 GPa. We discuss the influences of temperature, pressure, and the ratio of magnetite on the electrical conductivity of the samples. The percolation threshold in the magnetite-bearing sample has also been determined.

2. Experimental Procedures

2.1. Sample Preparation and Characterization

The natural gel-class olivine single crystals used in this study were gathered from nodular inclusions occurring in the alkali-rich basaltic region of the Xiaomaping area, Zhangjiakou City, Hebei Province, China. First, the raw samples were ultrasonically cleaned with pure water, acetone, and ethanol in turn. The samples were kept in a muffle furnace at 473 K for 24 h to remove absorbed water. Then, the olivine single crystal grains were crushed and ground into powdered samples with grain sizes of <20 μm for 5 h in the agate mortar. The raw powder of magnetite with grain sizes of <20 μm (99.99%; Aladdin, Shanghai, China). The mixture of powdered olivine with various volume percentages of magnetite (0, 3, 5, 7, 10, 20, and 100) was homogeneously mixed in the agate mortar for 2 h, hot-pressed and sintered in YJ-3000t multi-anvil high-pressure apparatus. Powder mixtures of reagent grade magnetite and well-characterized olivine were hot-pressed at 873 K and 1.0 GPa for 6 h. To avoid water absorption from the sample assembly during the high-pressure synthetic process,

double layers with a 0.1-mm thick copper sheet and a 0.025-mm nickel foil were adopted to completely seal the sample. A detailed sample preparation procedure for olivine aggregates has been previously described by Sun et al. [16].

The presence of small amounts of water in nominally anhydrous minerals has a considerable influence on the electrical conductivity of single crystal olivine and polycrystalline olivine aggregates at high temperature and high pressure [2,17,18]. To precisely determine the water content for the hot-pressed sintered olivine aggregates, we conducted the Fourier transform infrared (FTIR) analysis in the Key Laboratory of High-temperature and High-pressure Study of the Earth's Interior, Institute of Geochemistry, Chinese Academy of Sciences, Guiyang, China. The water contents of the samples before and after conductivity measurements were measured using a Fourier transform vacuum infrared spectrometer (Vertex-70V, Hyperion-1000 infrared microscope). Samples for IR analysis were cut and polished to a thickness of less than 150 μm . Each IR absorption measurement was conducted with unpolarized radiation from a mid-IR light source, a mercury-cadmium-telluride detector with a $100 \times 100 \mu\text{m}$ aperture, and a CaF_2 beam splitter. At least five spectra were obtained for each mineral from different areas of the surface and averaged to reduce the effects of the heterogeneous water distribution. Each spectrum was collected based on the total absorbance of OH groups between wavenumbers of $3000\text{--}3800 \text{ cm}^{-1}$ with 512 scans accumulated for each sample. On the basis of the typical hydrogen-related defect band in the range of $3000\text{--}3750 \text{ cm}^{-1}$, the water content in the sample was determined using an equation proposed by Paterson [19],

$$C_{\text{OH}} = \frac{B_i}{150\zeta} \int \frac{K(\nu)}{(3780 - \nu)} d\nu \quad (1)$$

where C_{OH} is the molar concentration of the OH group ($\text{H}/10^6 \text{ Si}$), B_i is the density factor ($43,900 \text{ cm H}/10^6 \text{ Silicon}$), ζ is the orientation factor of polycrystalline sample ($1/3$), and $K(\nu)$ is the absorption coefficient in cm^{-1} at the wavenumber ν (cm^{-1}). The integration was conducted over the range of $3000\text{--}3750 \text{ cm}^{-1}$.

To identify the phase structure and distribution of the magnetite-bearing olivine aggregates, the microstructure was investigated based on optical microscope and scanning electron microscopy (JSM-7800F) observations performed at the State Key Laboratory of Ore Deposit Geochemistry in the Institute of Geochemistry, Chinese Academy of Sciences, Guiyang, China.

2.2. High-Pressure Cell and Impedance Measurements

The in situ impedance spectroscopy measurements on the olivine aggregates at high pressure were conducted with the use of a Solartron-1260 impedance/gain-phase analyzer (Schlumberger, Houston, TX, USA) and a YJ-3000t multi-anvil apparatus. The measurement principles and experimental procedures have been previously reported by Dai et al. [20] and Hu et al. [21] in detail.

A detailed schematic diagram of the high-pressure cell used for electrical conductivity measurements, is illustrated in Figure 1. The YJ-3000t multi-anvil press was selected to generate the high-pressure environment, which was loaded by six symmetric cubic tungsten carbide anvils, each having a square edge length of 23.4 mm^2 . Before electrical conductivity measurements, all parts including the pressure medium of pyrophyllite, MgO, and Al_2O_3 insulation tubes were baked at 1173 K for 12 h in a muffle furnace. The cylindrical olivine aggregates sample with a diameter of 6.0 mm and a height of 6.0 mm was installed between the two symmetric disc-shaped metallic nickel electrodes (each electrode was 6.0 mm in diameter and 0.5 mm thickness), which were surrounded by the MgO tubes and the Al_2O_3 insulation sleeves. The heater was composed of three-layer stainless steel sheets with a total thickness of $\sim 0.5 \text{ mm}$. A Faraday shielding case consisting of a 0.025-mm metallic nickel foil was placed between the MgO tubes and the Al_2O_3 insulation sleeves, which was directly linked to the Earth line (*NiAl* earth line) to decrease signal interference during the impedance spectroscopy measurements. Temperatures with errors of $\pm 5 \text{ K}$ were measured using a *NiCr–NiAl* thermocouple. The pressure error was $\pm 0.1 \text{ GPa}$.

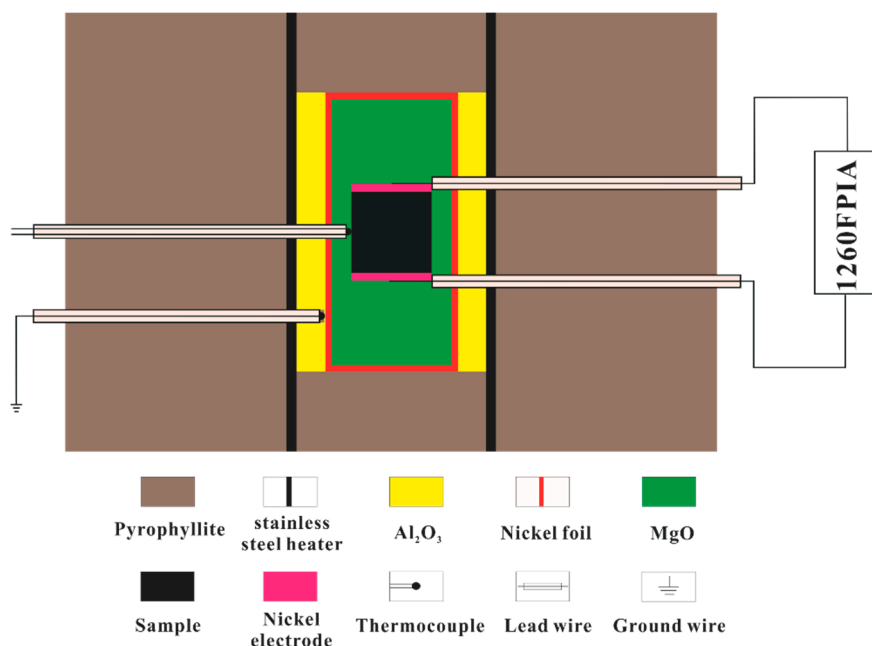


Figure 1. The cross-sectional experimental setup for electrical conductivity measurements at high temperature and high pressure.

The AC complex impedance spectroscopy measurements were performed on a system consisting of an impedance spectrometer (1260, Solartron) combined with a dielectric interface (1296, Solartron) within a frequency range of 10^{-1} to 10^6 Hz and at signal voltage of 1.0 V. One correspondent equivalent circuit that stands for the conduction process of sample was selected to fit the impedance semicircular arcs. To check for hysteresis effects in the electrical conductivity of the sample, each impedance spectrum was measured over three continuously heating and cooling cycles at a given temperature, pressure, and for the various ratios of magnetite in the olivine aggregates. During the first heating cycle, the sintered olivine aggregates was heated to the maximum designated temperature point of 1273 K in 50 K intervals at a given pressure and magnetite-bearing content. Electrical conductivity measurements were simultaneously recorded for at least 6–12 h at 1273 K to ensure that a constant equilibrium state was reached. The impedance spectra were then continuously collected over several subsequent heating–cooling cycles in the temperature range of 673–1273 K with the same procedure until reproducible resistance values were achieved. Therefore, for each experiment, a set of reproducible data that did not include the first and second heating–cooling cycles was chosen for the subsequent data fitting and analysis.

3. Results

In the experiments, the electrical conductivities of 5 vol. % magnetite-bearing olivine aggregates were measured at pressures of 1.0–3.0 GPa, temperatures of 873–1273 K, as well as for various contents of magnetite (0, 3, 5, 7, 10, 20, and 100 vol. %) at 2.0 GPa, and 873–1173 K.

The typical FTIR spectra of olivine aggregates in the wavenumbers range of $3000\text{--}4000\text{ cm}^{-1}$ before and after electrical conductivity measurements are shown in Figure 2. The water contents for the olivine aggregates before and after conductivity measurements were less than $\sim 8\text{ H}/10^6\text{ Silicon}$ (0.0001 wt %) and $\sim 12\text{ H}/10^6\text{ Silicon}$ (0.0001 wt %), respectively. Thus, we confirmed that the sample represents truly “dry” olivine aggregates. The variation of water content during the electrical conductivity measurements of the dry sample was no more than 15%.

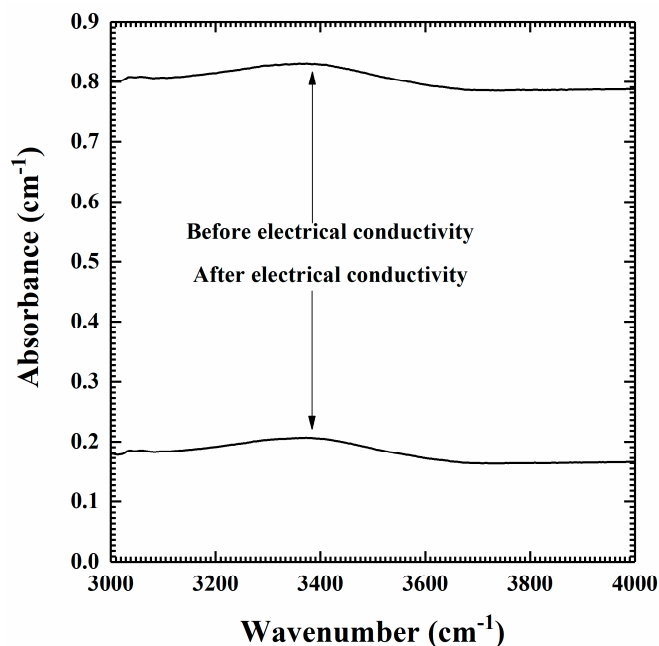


Figure 2. Fourier transform infrared (FTIR) spectra of olivine aggregates in the wavenumbers range of 3000–4000 cm^{-1} before and after electrical conductivity measurements.

Representative optical and back-scattered electron scanning electron microscopy images for the 5 vol. % magnetite-bearing recovered olivine aggregates before and after electrical conductivity measurements are shown in Figure 3. We found that there were no new observable phases except for the crystalline olivine aggregates and magnetite during the electrical conductivity measurements.

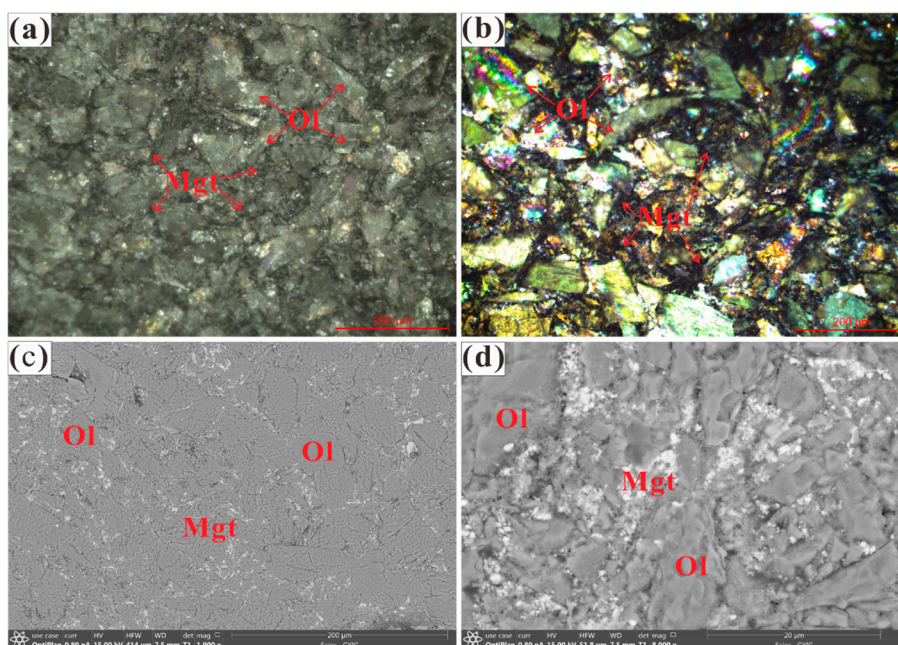


Figure 3. Representative microstructural observations of the recovered olivine aggregates with 5% volume fraction of magnetite. (a) and (b) microscopy images (plane-polarized reflected) acquired before and after the electrical conductivity measurements, respectively. (c) and (d) back-scattered electron images acquired with a scanning electron microscope before and after electrical conductivity measurements, respectively. Abbreviations are *Ol* olivine and *Mgt* magnetite.

Two sets of typical complex impedance spectra of the magnetite-free and 5 vol. % magnetite-bearing olivine aggregates at 2.0 GPa and 873–1273 K are shown in Figure 4. For the magnetite-free olivine aggregates, a relatively angular semicircular arc was observed within the whole frequency range of 10^{-1} – 10^6 Hz, which is representative of the bulk conduction processes of the sample. To obtain the electrical resistance results from the impedance spectroscopy data, an equilibrium circuit composed of a parallel non-ideal constant phase element (CPE) and resistance was used to fit the impedance semicircular arc for the magnetite-free sample. However, as for magnetite-bearing olivine aggregates, in addition to the bulk conduction of the sample, an additional electrical resistance appeared in the complex plane of the impedance spectroscopy. Thus, an equivalent circuit was selected to fit the AC impedance spectroscopy of the magnetite-bearing olivine aggregates based on the series connection of one resistance and one parallel resistance with the constant phase element (CPE). The results obtained under different pressures and the ratio of the magnetite-bearing olivine aggregates resembled those described above. The electrical conductivities of the samples were determined by the equation $\sigma = (L/S)/R$, where L/S is the geometric factor (L and S denote the length and cross-sectional area of the recovered sample (m) after the electrical conductivity measurements, respectively) and R is the bulk resistance of the sample (Ω). The dependence of the electrical conductivity with temperature for olivine aggregates can be expressed by the Arrhenius relation,

$$\sigma = \sigma_0 \exp\left(-\frac{\Delta H}{k_b T}\right) \quad (2)$$

where σ is the electrical conductivity (S/m), σ_0 is the pre-exponential factor (S/m), T is the absolute temperature (K), k_b is the Boltzmann constant (eV/K), and ΔH is the activation enthalpy (eV). This parameter can be defined as a function of pressure (P) by the equation $\Delta H = \Delta U + P\Delta V$, where ΔU and ΔV represent the activation energy (eV) and the activation volume (cm^3/mole), respectively.

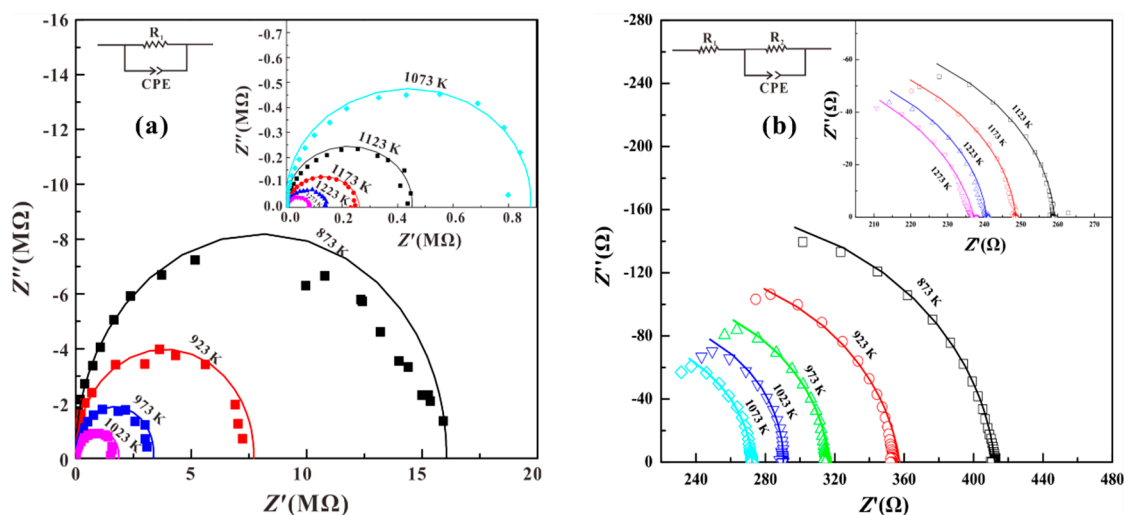


Figure 4. Two sets of typical complex impedance spectra of the magnetite-free (a) and 5 vol. % magnetite-bearing (b) olivine aggregates at frequencies from 10^{-1} to 10^6 Hz (right to left), obtained under conditions of 2.0 GPa and 873–1273 K. Z' and Z'' are the real and imaginary parts of the complex impedance, respectively. The equilibrium circuit was made up of a parallel non-ideal constant phase element (CPE) and the resistance was selected to fit the impedance semicircular arc for magnetite-free aggregates. As for the magnetite-bearing samples, the complex impedance spectra were fitted using an equivalent circuit of a series connection of one resistance and the constant phase element with a resistance in parallel.

To determine the effects of hysteresis, the electrical conductivities of magnetite-free and 5 vol. % magnetite-bearing olivine aggregates for three heating–cooling cycles at a pressure of 2.0 GPa are

shown in Figure 5. The electrical conductivities of the sample were acquired at a constant equilibrium state after the second cooling cycle, which was reached after a sufficiently long equilibrium time (at least 6–12 h) at the maximum measured temperature of 1273 K. Overall, the electrical conductivity of the magnetite-free and magnetite-bearing olivine in the third heating–cooling cycles was lower than the values of other two heating–cooling cycles, which might be related to the disequilibrium of thermal transfer, disequilibrium of texture and moisture of the sample. The influence of pressure on the 5 vol. % magnetite-bearing olivine aggregates in the temperature range of 873–1273 K is shown in Figure 6, and the fitting parameters of the Arrhenius relation are listed in Table 1. Figure 7 shows the relationship between the electrical conductivity and the ratio of various magnetite-bearing samples at 2.0 GPa and 873–1273 K.

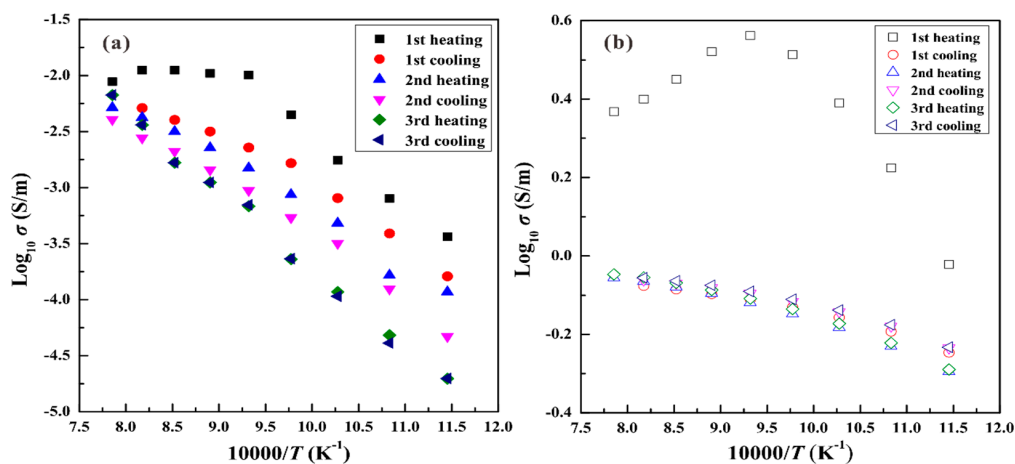


Figure 5. Electrical conductivities of the magnetite-free and 5 vol. % magnetite-bearing olivine aggregates as a function of the reciprocal temperatures during three heating–cooling cycles at 2.0 GPa. At 1273 K, each conductivity experiment was performed for at least 6–12 h in order to avoid the effects of disequilibrium of the thermal transfer, disequilibrium of texture and moisture of the sample. Three heating–cooling cycles over the temperature range of 673–1273 K were continuously measured for magnetite-free (a) and magnetite-bearing (b) samples, and electrical conductivities of samples in the third cycles were reproducible.

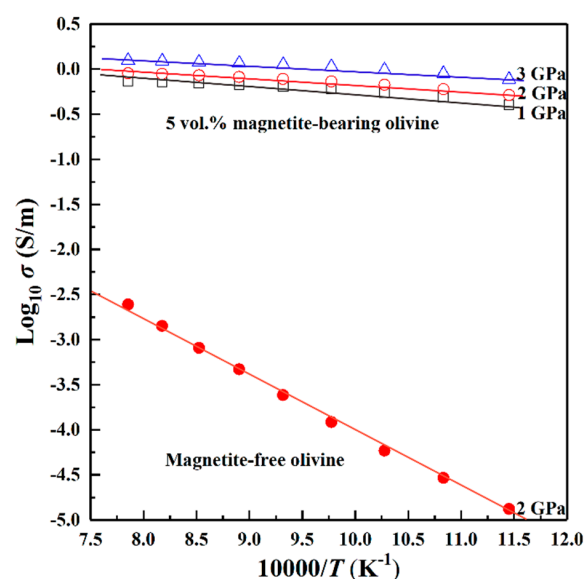
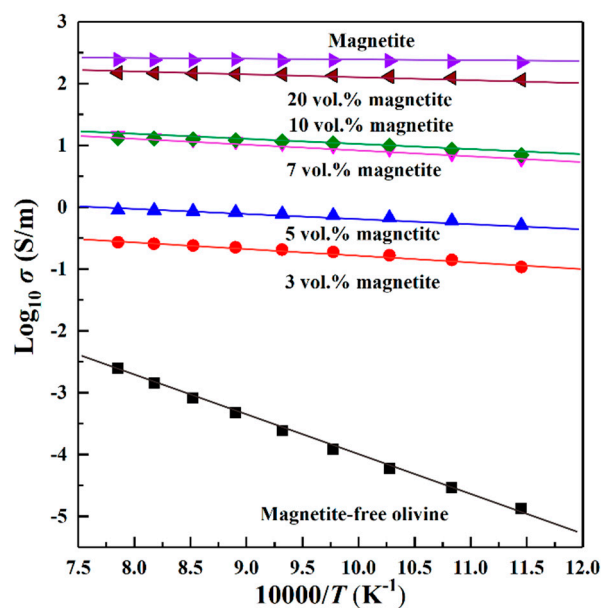


Figure 6. Influence of pressure on the electrical conductivity of 5 vol. % magnetite-bearing olivine aggregates in the temperature range of 873–1173 K. The electrical conductivity of the magnetite-free sample is presented for comparison at 2.0 GPa.

Table 1. Fitted parameters of the Arrhenius relation for the electrical conductivity of the magnetite-free and magnetite-bearing olivine aggregates at 1.0–3.0 GPa and 873–1273 K.

| Run No. | <i>P</i> (GPa) | ϕ_{mgt} (vol. %) ^a | Log σ_0 | ΔH (eV) | γ^2 (b) |
|---------|----------------|---|----------------|-----------------|----------------|
| DL1807 | 2.0 | 0 | 1.27 ± 0.03 | 1.27 ± 0.01 | 99.76 |
| DL1816 | 2.0 | 3 | 0.28 ± 0.03 | 0.21 ± 0.02 | 96.92 |
| DL1820 | 1.0 | 5 | 0.44 ± 0.02 | 0.14 ± 0.02 | 98.49 |
| DL1824 | 2.0 | 5 | 0.49 ± 0.02 | 0.13 ± 0.01 | 99.21 |
| DL1826 | 3.0 | 5 | 0.56 ± 0.01 | 0.11 ± 0.01 | 99.36 |
| DL1829 | 2.0 | 7 | 1.97 ± 0.01 | 0.20 ± 0.02 | 99.41 |
| DL1831 | 2.0 | 10 | 1.72 ± 0.03 | 0.15 ± 0.01 | 97.94 |
| DL1832 | 2.0 | 20 | 2.40 ± 0.02 | 0.06 ± 0.01 | 98.92 |
| DL1836 | 2.0 | 100 | 2.47 ± 0.02 | 0.02 ± 0.01 | 96.21 |

Note: a, ϕ_{mgt} stands for the volume fraction of magnetite in the olivine aggregates sample, b stands for the degree of linear correlation in the fitted Arrhenius relation.

**Figure 7.** Effect of the magnetite volume fraction on the electrical conductivity of olivine aggregates at 2.0 GPa and 873–1173 K.

4. Discussion

4.1. Influence of Pressure on the Electrical Conductivity

With increasing pressure, the electrical conductivity of 5 vol. % magnetite-bearing olivine aggregates increased, and the logarithm of the pre-exponential factor ($\text{Log } \sigma_0$) also increased from 0.44 to 0.56 (see Table 1). Accordingly, the activation enthalpy (ΔH) decreased slightly from 0.14 to 0.11 eV. In comparison, a relatively large activation enthalpy value of 1.27 eV was obtained for the anhydrous magnetite-free olivine aggregates at 2.0 GPa, which is in good agreement with previous results for polycrystalline olivine compacts and single crystal olivine obtained by Dai et al., Poe et al., Xu et al., and Yang [22–25]. Just as described by Dai and Karato [26], there are three main influential factors, namely water content, iron content, and pressure, which are likely to contribute to the feeble differences between the previously obtained activation enthalpies of dry magnetite-free polycrystalline olivine aggregates and ours. Furthermore, the activation energy and the activation volume of the charge carriers for the 5 vol. % magnetite-bearing sintered olivine aggregates at atmospheric pressure were calculated as $\Delta U = \sim 0.16 \pm 0.04$ eV and $\Delta V = \sim -1.50 \pm 0.04$ cm³/mole respectively. A linear relationship between $\text{Log } \sigma$ and the reciprocal temperature at room pressure was also extrapolated from Figures 6 and 7. We attribute the positive dependence of the electrical conductivity on the pressure

of the samples to more effective formation and migration of defects in small polaron conduction mechanism at higher pressure. In addition, the obtained negative value of the activation volume for the magnetite-bearing sample ($\Delta V = -1.50 \pm 0.04 \text{ cm}^3/\text{mole}$) is similar to previously obtained results for some other representative anhydrous iron-containing silicate minerals and rocks in the Earth's mantle and subduction zone at high temperature and high pressure, e.g. hot-pressed sintered polycrystalline olivine aggregates, natural eclogite, silicate perovskite and magnesiowüstite, as reported by Dai et al., Dobson, Goddat et al. and Xu et al. [22,27–30].

4.2. Influence of Magnetite Volume Fraction on Electrical Conductivity

Figure 7 shows the relationship between the electrical conductivity and the ratio of the various magnetite-bearing samples at 2.0 GPa and 873–1273 K. The dependence of the activation enthalpy on the volume fraction of magnetite is shown in detail in Figure 8. As the magnetite fraction increases from 3 to 100 vol. %, the electrical conductivity of the olivine aggregates increased, and the logarithmic pre-exponential factor increased from 0.28 to 2.47, whereas the activation enthalpy tended to decrease from 0.21 to 0.02 eV.

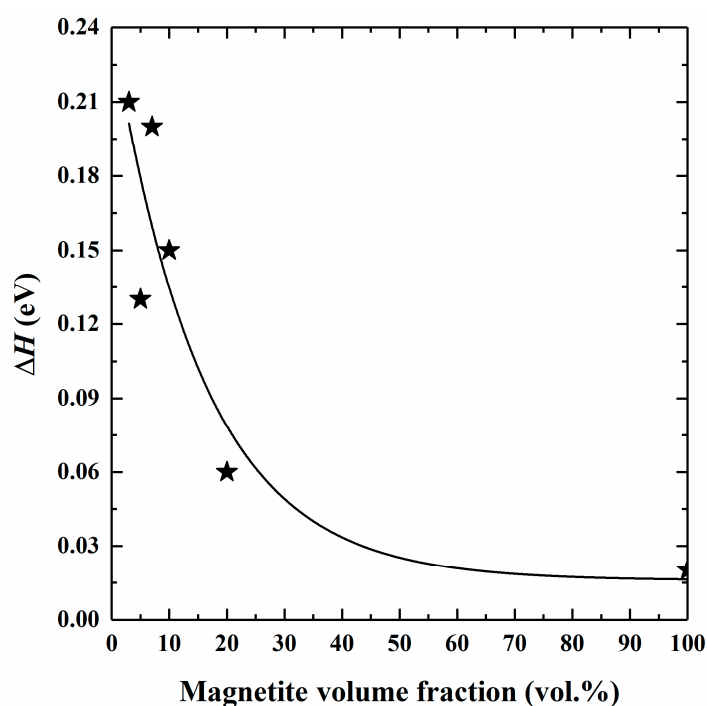


Figure 8. Dependence of the activation enthalpy (ΔH) on the volume fraction of magnetite in olivine aggregates at 2.0 GPa and 873–1173 K.

To further assess the influence of the individual volume fraction of magnetite on the electrical conductivity of olivine aggregates, we examined the electrical conductivities under two experimental boundary temperature conditions (873 K and 1273 K) at 2.0 GPa, as shown in Figure 9. The electrical conductivity of the olivine aggregates clearly increased by at least four orders of magnitude at 873 K and two orders of magnitude at 1273 K when the magnetite volume fraction was varied from 0 to 5 vol. %. The effect of magnetite on the electrical conductivity showed a phenomenon of percolation threshold, which can be used to describe the formation of interconnected characteristics in the high conductive impurity at high-temperature and high-pressure conditions [9–12]. If the concentration of high conductive impurities into the olivine aggregates is enough, a fully interconnected high conductive pathway is formed in the sample resulting in a step increase of the electrical conductivity several orders of magnitude. In this case, the corresponding concentration of the impurity material at the electrical conductivity jump is denoted as the percolation threshold value. Our electrical

conductivity results, displayed in Figure 9 show that the 5% volume fraction of magnetite is the percolation threshold value in the olivine aggregates at 2 GPa. In addition, the 5% volume fraction of magnetite also exhibited an interconnected characteristics by the above-mentioned the microstructural observations from the optical microscope and scanning electron microscopy, as shown in Figure 3.

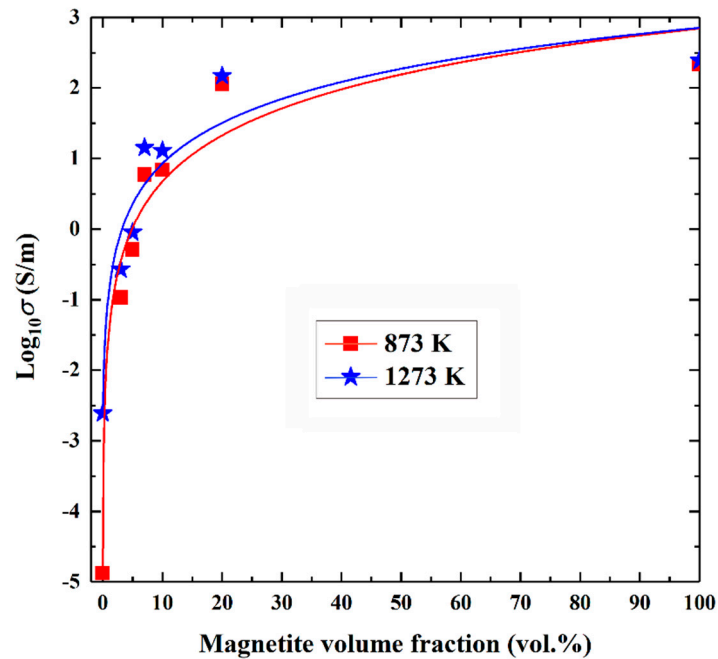


Figure 9. Influence of the magnetite volume fraction on the electrical conductivity of olivine aggregates. Electrical conductivities were obtained under two experimental boundary temperature conditions (873 K and 1273 K) at 2.0 GPa.

4.3. Conduction Mechanism

The electrical conductivity of the silicate mineral and rock can be described as the total contribution from each individual charge carrier (or defect) species as follows,

$$\sigma = \sum_j q_j n_j \mu_j \quad (3)$$

where q_j is the effective charge ($q = ze$), n_j is the concentration of point defects for the j -th type of charge carrier, and μ_j is the mobility ($\mu_j = v/E$, where v is the drift velocity of the particle and E is the applied electric field). Each corresponding conduction mechanism depends on the activation enthalpy of the charge-carrier mobility, which can be distinguished from the different activation enthalpies in the designated temperature range of the Arrhenius relation diagram. Considering our new results for magnetite-free and magnetite-bearing olivine aggregates, the Arrhenius relation was found between the electrical conductivity and temperature; thus, it is possible that only one individual conduction mechanism is active at conditions of 873–1273 K and 1.0–3.0 GPa.

Previous available results have confirmed that there are three main conduction mechanisms operating in olivine aggregates at high temperature and high pressure (i.e., hydrogen-related defects, small polaron and ionic conduction) [31,32]. The conduction mechanism of hydrogen-related defects occurs owing to small amounts of hydrogen in the nominally anhydrous olivine and its high-pressure polymorph, which is characterized by a relatively low activation enthalpy (<1.0 eV) and a negative exponential dependence of the electrical conductivity on the oxygen fugacity (−0.060) [26,33]. The electrical transport process can be described by the ionization reaction,



where $(2\text{H})_{\text{M}}^{\times}$ denotes two protons in the crystalline lattice at M-site, H'_{M} denotes a proton trapped at an M-site vacancy, H^{\bullet} denotes a free proton and M is the iron or magnesium ion of ferromagnesian silicate mineral. Although the presently obtained values of 0.02–0.21 eV for the activation enthalpies of the magnetite-bearing samples are close to those of single-crystal, polycrystalline, and hot-pressed sintered hydrous olivines [2,24,25,34], the conduction mechanism of the hydrogen-related defects is not possible in our case because the olivine aggregates are anhydrous, as confirmed by the FTIR spectroscopy results (Figure 2). Magnesium and oxygen vacancy ionic conduction is one of the main conduction mechanisms in fayalite-rich and forsterite-rich olivines at experimental temperatures higher than 1473 K [32,35,36]. As pointed out by Yoshino et al. [32], the ionic conduction in olivine aggregates is characterized by a positive value on the order from several to several tens of cm^3/mole , a relatively high activation energy (>1.8 eV), and a negative pressure dependence of the electrical conductivity at high pressure. Therefore, we conclude that our electrical conductivity data for magnetite-bearing olivine aggregates does not include significant contributions from the hydrogen-related defects or ionic conduction mechanisms.

The small polaron is a primary candidate for electrical conduction mechanism and our obtained results also suggest this mechanism operates in the magnetite-bearing olivine aggregates, which includes a negative activation volume ($-1.50 \text{ cm}^3/\text{mole}$), a low activation enthalpy (0.06–0.21 eV), and a positive dependence of the electrical conductivity on pressure. The hopping of small polaron between ferrous and ferric iron is thought to occur by the point defect reaction [30,35,36],



where $\text{Fe}_{\text{Mg}}^{\times}$ and $\text{Fe}_{\text{Mg}}^{\bullet}$ are divalent and trivalent iron ions at the site of magnesium ions in the lattice, respectively. The main charge carrier is the small polaron, i.e., $\text{Fe}_{\text{Mg}}^{\bullet}$ (Fe^{3+} at Mg site), which contributes to conduction by hopping of the electron (e) between $\text{Fe}_{\text{Mg}}^{\times}$ and $\text{Fe}_{\text{Mg}}^{\bullet}$. Many high-pressure experimental reports have confirmed the small polaron as the main conduction mechanism for the endmember of magnetite-free olivine aggregates [18,22,23,30,35,36]. In addition, another endmember of magnetite with an inverse spinel structure is also well known for its electronic hopping between ferrous and ferric iron octahedral sites at a pressure range of 0–20 GPa [37]. According to the P – T phase diagram for magnetite reported by Schollenbruch et al. [38], magnetite is always stable as a spinel-structured phase at conditions of 1.0–3.0 GPa and 873–1273 K. Thus, we conclude that the small polaron is the main electrical conduction mechanism for dry sintered olivine aggregates with various contents of magnetite (0, 3, 5, 7, 10, 20, and 100 vol. %). Yamanaka et al. [13] reported the formation of a solid solution between fayalite and magnetite, and found that the mixed conduction mechanism of small polaron hopping and silicon vacancies at octahedral sites can operate in the $\text{Fe}_{3-\delta}\text{Si}_{\delta}\text{O}_4$ solid solution of olivine, which is consistent with our present results.

5. Implications

The experimental results of this study show that the electrical conductivity of olivine aggregates increases as the volume fraction of magnetite increases, and at 2.0 GPa, the interconnected magnetite percolation threshold has a particularly high electrical conductivity value at a relatively low ~5% volume fraction. Previous mineralogical, petrological, and geochemical evidences have shown that the magnetite with an inverse spinel structure was intergrown with or exsolved from olivine in a variety of geotectonic environments, such as the Dabie–Sulu ultrahigh-pressure metamorphic belt and Luobusha of Southern Tibet [14,15]. In most cases, the available volume fraction percentage of magnetite lamellae in natural olivine was not more than 1.5 vol. % from the crust–mantle origin [14,15,39,40]. Although some regional clustering effects might result in a heterogeneous distribution of magnetite, the present measurement technique of long-period field magnetotelluric observation is difficult to survey the regional clustering phenomenon of magnetite. Therefore, the considerable increase in the electrical conductivity of the 5 vol. % interconnected magnetite-bearing olivine aggregates cannot explain

the high electrical conductivity anomalies in magnetotelluric and electromagnetic observation data (10^{-2} – 10^{-1} S/m) of the stable continental crust and asthenosphere of the Earth's upper mantle [41–44]. Another potentially related high conductivity anomaly zone at depths beyond 70 km exists at the slab–mantle wedge interface in the subduction zone [3,45–48]. The serpentinization of peridotite might be one candidate to explain the high electrical conductivity and the low-velocity seismic wave anomalies with a high Poisson's ratio in this region of the mantle wedge. Kawano et al. [49] reported on the electrical conductivities of serpentinite with various amounts of magnetite (5,10,20,30, and 50 vol. %) during shear deformation process and confirmed that at least a 25 vol. % magnetite was required to achieve interconnection of magnetite in serpentinite at 1.0 GPa and 750 K. Clearly, this value cannot correspond to the conditions of a really regional geotectonic environment, which is impossible to contain such high volume fractions of magnetite at that depth range of the slab–mantle wedge interface of the subduction zone. In consideration of the crystal structure and its phase stability in the solid solution of spinel (or spinelloid)-structured minerals and the high-pressure polymorphs of olivine (such as wadsleyite and ringwoodite) [50–53], further research is required under higher temperature and pressure conditions to explore the influence of the magnetite fraction on the electrical conductivity of the minerals and rocks of the mantle transition zone in the future. In summary, the presence of an interconnected high conductivity impurity phase in olivine aggregates with the 5% volume fraction of magnetite is unlikely to account for the high conductivity anomaly in the deep Earth's interior. Other mechanisms are necessary to explain this phenomenon, such as water-bearing (or brine-bearing) fluid, dehydration (or dehydrogenation) of mineral, partial melting or hydrogen of nominally anhydrous minerals.

Author Contributions: Lidong Dai and Haiying Hu (designing the project). Lidong Dai (writing the initial draft of the work and the final paper). Lidong Dai, Haiying Hu, Wenqing Sun, Heping Li, Changcai Liu and Mengqi Wang (interpreting the results). Wenqing Sun, Changcai Liu and Mengqi Wang (conducting high-P experiments). Lidong Dai and Changcai Liu (performing and interpreting the optical microscope and scanning electron microscope analyses). All authors discussed the results and commented on the manuscript.

Funding: This research was financially supported by the strategic priority Research Program (B) of the Chinese Academy of Sciences (Grant No. 18010401), Key Research Program of Frontier Sciences of CAS (Grant No. QYZDB-SSW-DQC009), “135” Program of the Institute of Geochemistry of CAS, Hundred Talents Program of CAS and NSF of China (Grant Nos. 41474078, 41774099 and 41772042).

Acknowledgments: We thank the guest editor of Professor Xi Liu from Peking University for kindly handling our paper, and as well as two anonymous reviewers for constructive and enlightened comments and suggestions in the revising process.

Conflicts of Interest: The authors declare no conflict of interest.

References

1. Huang, X.; Xu, Y.; Karato, S. Water content in the transition zone from electrical conductivity of wadsleyite and ringwoodite. *Nature* **2005**, *434*, 746–749. [[CrossRef](#)] [[PubMed](#)]
2. Wang, D.; Mookherjee, M.; Xu, Y.; Karato, S. The effect of water on the electrical conductivity of olivine. *Nature* **2006**, *443*, 977–980. [[CrossRef](#)] [[PubMed](#)]
3. Manthilake, G.; Bolfan-Casanova, N.; Novella, D.; Mookherjee, M.; Andrault, D. Dehydration of chlorite explains anomalously high electrical conductivity in the mantle wedges. *Sci. Adv.* **2016**, *2*, e1501631. [[CrossRef](#)] [[PubMed](#)]
4. Chen, S.; Guo, X.; Yoshino, T.; Jin, Z.; Li, P. Dehydration of phengite inferred by electrical conductivity measurements: Implication for the high conductivity anomalies relevant to the subduction zones. *Geology* **2018**, *46*, 11–14. [[CrossRef](#)]
5. Gaillard, F.; Malki, M.; Iacono-Marziano, G.; Pichavant, M.; Scaillet, B. Carbonatite melts and electrical conductivity in the asthenosphere. *Science* **2008**, *322*, 1363–1365. [[CrossRef](#)] [[PubMed](#)]
6. Laumonier, M.; Farla, R.; Frost, D.; Katsura, T.; Marquardt, K.; Bouvier, A.; Baumgartner, L. Experimental determination of melt interconnectivity and electrical conductivity in the upper mantle. *Earth Planet. Sci. Lett.* **2017**, *463*, 286–297. [[CrossRef](#)]

7. Hu, H.; Dai, L.; Li, H.; Sun, W.; Li, B. Effect of dehydrogenation on the electrical conductivity of Fe-bearing amphibole: Implications for high conductivity anomalies in subduction zones and continental crust. *Earth Planet. Sci. Lett.* **2018**, *498*, 27–37. [[CrossRef](#)]
8. Dai, L.; Karato, S. High and highly anisotropic electrical conductivity of the asthenosphere due to hydrogen diffusion in olivine. *Earth Planet. Sci. Lett.* **2014**, *408*, 79–86. [[CrossRef](#)]
9. Yoshino, T.; Walter, M.; Katsura, T. Core formation in planetesimals triggered by permeable flow. *Nature* **2003**, *422*, 154–157. [[CrossRef](#)]
10. Watson, H.; Roberts, J.; Tyburczy, J. Effect of conductive impurities on electrical conductivity in polycrystalline olivine. *Geophys. Res. Lett.* **2010**, *37*, L02302. [[CrossRef](#)]
11. Wang, D.; Karato, S.; Jiang, Z. An experimental study of the influence of graphite on the electrical conductivity of olivine aggregates. *Geophys. Res. Lett.* **2013**, *40*, 2028–2032. [[CrossRef](#)]
12. Zhang, Z.; Pommier, A. Electrical investigation of metal-olivine systems and application to the deep interior of Mercury. *J. Geophys. Res. Planets* **2017**, *122*, 2702–2718. [[CrossRef](#)]
13. Yamanaka, T.; Shimazu, H.; Ota, K. Electric conductivity of Fe₂SiO₄–Fe₃O₄ spinel solid solutions. *Phys. Chem. Miner.* **2001**, *28*, 110–118. [[CrossRef](#)]
14. Zhang, R.; Shu, J.; Mao, H.; Liou, J. Magnetite lamellae in olivine and clinohumite from Dabie UHP ultramafic rocks, central China. *Am. Mineral.* **1999**, *84*, 564–569. [[CrossRef](#)]
15. Hu, J.; Mao, S.; Du, G.; Wu, Y.; Zhang, P. A new thermodynamic analysis of the intergrowth of hedenbergite and magnetite with Ca-Fe-rich olivine. *Am. Mineral.* **2001**, *96*, 599–608. [[CrossRef](#)]
16. Sun, W.; Dai, L.; Li, H.; Hu, H.; Wu, L.; Jiang, J. Electrical conductivity of mudstone (before and after dehydration at high PT) and a test of high conductivity layers in the crust. *Am. Mineral.* **2017**, *102*, 2450–2456. [[CrossRef](#)]
17. Dai, L.; Karato, S. The effect of pressure on the electrical conductivity of olivine under the hydrogen-rich conditions. *Phys. Earth Planet. Inter.* **2014**, *232*, 51–56. [[CrossRef](#)]
18. Dai, L.; Karato, S. Influence of FeO and H on the electrical conductivity of olivine. *Phys. Earth Planet. Inter.* **2014**, *237*, 73–79. [[CrossRef](#)]
19. Paterson, M. The determination of hydroxyl by infrared absorption in quartz, silicate glasses, and similar materials. *Bull. Mineral.* **1982**, *105*, 20–29.
20. Dai, L.; Li, H.; Hu, H.; Shan, S.; Jiang, J.; Hui, K. The effect of chemical composition and oxygen fugacity on the electrical conductivity of dry and hydrous garnet at high temperatures and pressures. *Contrib. Mineral. Petrol.* **2012**, *163*, 689–700. [[CrossRef](#)]
21. Hu, H.; Dai, L.; Li, H.; Hui, K.; Sun, W. Influence of dehydration on the electrical conductivity of epidote and implications for high-conductivity anomalies in subduction zones. *J. Geophys. Res. Solid Earth* **2017**, *122*, 2751–2762. [[CrossRef](#)]
22. Xu, Y.; Shankland, T.; Duba, A. Pressure effect on electrical conductivity of mantle olivine. *Phys. Earth Planet. Inter.* **2000**, *118*, 149–161. [[CrossRef](#)]
23. Dai, L.; Li, H.; Li, C.; Hu, H.; Shan, S. The electrical conductivity of dry polycrystalline olivine compacts at high temperatures and pressures. *Mineral. Mag.* **2010**, *74*, 849–857. [[CrossRef](#)]
24. Poe, B.; Romano, C.; Nestola, F.; Smyth, J.R. Electrical conductivity anisotropy of dry and hydrous olivine at 8 GPa. *Phys. Earth Planet. Inter.* **2010**, *181*, 103–111. [[CrossRef](#)]
25. Yang, X. Orientation-related electrical conductivity of hydrous olivine, clinopyroxene and plagioclase and implications for the structure of the lower continental crust and uppermost mantle. *Earth Planet. Sci. Lett.* **2012**, *317*, 241–250. [[CrossRef](#)]
26. Dai, L.; Karato, S. Influence of oxygen fugacity on the electrical conductivity of hydrous olivine: Implications for the mechanism of conduction. *Phys. Earth Planet. Inter.* **2014**, *232*, 57–60. [[CrossRef](#)]
27. Dai, L.; Hu, H.; Li, H.; Wu, L.; Hui, K.; Jiang, J.; Sun, W. Influence of temperature, pressure, and oxygen fugacity on the electrical conductivity of dry eclogite, and geophysical implications. *Geochem. Geophys. Geosyst.* **2016**, *17*, 2394–2407. [[CrossRef](#)]
28. Dobson, D.; Richmond, N.; Brodholt, J. A high-temperature electrical conduction mechanism in the lower mantle phase (Mg,Fe)_{1-x}O. *Science* **1997**, *275*, 1779–1781. [[CrossRef](#)]
29. Dobson, D.; Brodholt, J. The electrical conductivity of the lower mantle phase magnesiowustite at high temperatures and pressures. *J. Geophys. Res. Solid Earth* **2000**, *105*, 531–538. [[CrossRef](#)]
30. Goddat, A.; Peyronneau, J.; Poirier, J. Dependence on pressure of conduction by hopping of small polarons in minerals of the Earth's lower mantle. *Phys. Chem. Minerals* **1999**, *27*, 81–87. [[CrossRef](#)]

31. Karato, S. Theory of isotope diffusion in a material with multiple species and its implications for hydrogen-enhanced electrical conductivity in olivine. *Phys. Earth Planet. Inter.* **2014**, *219*, 49–54. [[CrossRef](#)]
32. Yoshino, T.; Zhang, B.; Rhymer, B.; Zhao, C.; Fei, H. Pressure dependence of electrical conductivity in forsterite. *J. Geophys. Res. Solid Earth* **2017**, *122*, 158–171. [[CrossRef](#)]
33. Dai, L.; Karato, S. Electrical conductivity of wadsleyite at high temperatures and high pressures. *Earth Planet. Sci. Lett.* **2009**, *287*, 277–283. [[CrossRef](#)]
34. Yoshino, T.; Matsuzaki, T.; Yamashita, S.; Katsura, T. Hydrous olivine unable to account for conductivity anomaly at the top of the asthenosphere. *Nature* **2006**, *443*, 973–976. [[CrossRef](#)] [[PubMed](#)]
35. Omura, K.; Kurita, K.; Kumazawa, M. Experimental study of pressure dependence of electrical conductivity of olivine at high temperatures. *Phys. Earth Planet. Inter.* **1989**, *57*, 291–303. [[CrossRef](#)]
36. Schock, R.; Duba, A.; Shankland, T. Electrical conduction in olivine. *J. Geophys. Res.* **1989**, *94*, 5829–5839. [[CrossRef](#)]
37. Morris, E.; Williams, Q. Electrical resistivity of Fe₃O₄ to 48 GPa: Compression-induced changes in electron hopping at mantle pressures. *J. Geophys. Res. Solid Earth* **1997**, *102*, 18139–18148. [[CrossRef](#)]
38. Schollenbruch, K.; Woodland, A.; Frost, D.; Langenhorst, F. Detecting the spinel–post-spinel transition in Fe₃O₄ by in situ electrical resistivity measurements. *High Press. Res.* **2009**, *29*, 520–524. [[CrossRef](#)]
39. Naemura, K.; Hirajima, T.; Svojtka, M. The pressure–temperature path and the origin of phlogopite in spinel–garnet peridotites from the Blanský les Massif of the Moldanubian zone, Czech Republic. *J. Petrol.* **2009**, *50*, 1795–1827. [[CrossRef](#)]
40. Khedr, M.; Arai, S. Composite origin of magnetite deposits hosted in Oman peridotites: Evidence for iron mobility during serpentinization. *Ore Geol. Rev.* **2018**, *101*, 180–198. [[CrossRef](#)]
41. Evans, R.; Hirth, G.; Baba, K.; Forsyth, D.; Chave, A.; Makie, R. Geophysical evidence from the MELT area for compositional control on oceanic plates. *Nature* **2005**, *437*, 249–252. [[CrossRef](#)] [[PubMed](#)]
42. Yang, X.; McCammon, C. Fe³⁺-rich augite and high electrical conductivity in the deep lithosphere. *Geology* **2012**, *40*, 131–134. [[CrossRef](#)]
43. Naif, S.; Key, K.; Constable, S.; Evans, R. Melt-rich channel observed at the lithosphere–asthenosphere boundary. *Nature* **2013**, *495*, 356–359. [[CrossRef](#)] [[PubMed](#)]
44. Guo, X.; Yoshino, T.; Shimojuku, A. Electrical conductivity of albite–(quartz)–water and albite–water–NaCl systems and its implication to the high conductivity anomalies in the continental crust. *Earth Planet. Sci. Lett.* **2015**, *412*, 1–9. [[CrossRef](#)]
45. Wannamaker, P.; Caldwell, T.; Jiracek, G.; Maris, V.; Hill, G.; Ogawa, Y.; Bibby, H.; Bennie, S.; Heise, W. Fluid and deformation regime of an advancing subduction system at Marlborough, New Zealand. *Nature* **2009**, *460*, 733–736. [[CrossRef](#)] [[PubMed](#)]
46. Guo, X.; Yoshino, T.; Katayama, I. Electrical conductivity anisotropy of deformed talc rocks and serpentinites at 3 GPa. *Phys. Earth Planet. Inter.* **2011**, *188*, 69–81. [[CrossRef](#)]
47. Worzewski, T.; Jegen, M.; Kopp, H.; Brasse, H.; Castillo, W. Magnetotelluric image of the fluid cycle in the Costa Rican subduction zone. *Nat. Geosci.* **2011**, *4*, 108–111. [[CrossRef](#)]
48. Hasegawa, A. Seismic imaging of mantle wedge corner flow and arc magmatism. *Proc. Jpn. Acad.* **2018**, *94*, 217–234. [[CrossRef](#)]
49. Kawano, S.; Yoshino, T.; Katayama, I. Electrical conductivity of magnetite-bearing serpentinite during shear deformation. *Geophys. Res. Lett.* **2012**, *39*, L20313. [[CrossRef](#)]
50. Liu, X.; Xiong, Z.; Shieh, S.; He, Q.; Deng, L.; Zhang, Y.; Chang, L.; Wang, F.; Hong, X.; Chen, Z. Non-monotonic compositional dependence of isothermal bulk modulus of the (Mg_{1-x}Mn_x)Cr₂O₄ spinel solid solutions, and its origin and implication. *Solid Earth Sci.* **2016**, *1*, 89–100. [[CrossRef](#)]
51. Liu, L.; Liu, X.; Bao, X.; He, Q.; Yan, W.; Ma, Y.; He, M.; Tao, R.; Zou, R. Si-disordering in MgAl₂O₄-spinel under high PT conditions, with implications for Si-Mg disorder in Mg₂SiO₄-Ringwoodite. *Minerals* **2018**, *8*, 210. [[CrossRef](#)]
52. Mi, Z.; Shi, W.; Zhang, L.; Shieh, S.; Liu, X. Equation of state of a natural chromian spinel at ambient temperature. *Minerals* **2018**, *8*, 591. [[CrossRef](#)]
53. Woodland, A.; Angel, R. Crystal structure of a new spinelloid with the wadsleyite structure in the system Fe₂SiO₄-Fe₃O₄ and implications for the Earth’s mantle. *Am. Mineral.* **1998**, *83*, 404–408. [[CrossRef](#)]

